Probabilistic Flutter Analysis of a Cantilever Wing

Sandeep Kumar, Amit K. Onkar, and M. Manjuprasad

Abstract A probabilistic flutter analysis of geometrically coupled cantilever wing is carried out using first-order perturbation approach by considering bending and torsional rigidities as Gaussian random variables. The unsteadiness in the aerodynamic flow is modeled using Theodorsen's thin airfoil theory. The probabilistic response of the wing is obtained in terms of mean, standard deviation, and coefficient of variation (COV) of real and imaginary parts of the eigenvalues at various free stream velocities. The perturbation results are also compared with Monte Carlo simulations. It is observed that the probabilistic response obtained from the perturbation approach is very accurate up to 7% COV in bending rigidity but in the case of torsional rigidity, it starts losing accuracy after 3%.

1 Introduction

In the design of aircraft, one of the critical failure phenomena, which happens in the aeroelastic system due to the fact that power pumped by aerodynamic flow is not completely able to be dissipated by the dissipative mechanism of the aeroelastic system, and the structure fails catastrophically due to diverging large amplitude vibrations. The flow velocity at which there is power balance, is called flutter velocity. In general, the material properties of the structure is not unique, and it depends on various factors such as method of manufacturing, method of testing and

S. Kumar · A. K. Onkar (✉) · M. Manjuprasad
Academy of Scientific and Innovative Research (AcSIR), Bengaluru 560017, Karnataka, India
e-mail: aeroamit@nal.res.in

S. Kumar
e-mail: sandeepk@alumni.iitg.ac.in

M. Manjuprasad
e-mail: manjuprasad@nal.res.in

CSIR-National Aerospace Laboratories, Bengaluru 560017, Karnataka, India

test conditions, human errors in calculation, etc. So the material properties must be modeled as stochastic parameters in order to get more realistic results.

Pettit [1] showed the importance and challenges of uncertainty quantification in aeroelasticity and potential future application of uncertainty-based aircraft design over the conventional factor of safety-based design. Kurdi et al. [2] considered the box type of Goland wing with spars and ribs, and their thickness and area were considered as Gaussian random variables. For probabilistic response analysis, a Monte Carlo Simulation (MCS) approach was used where free vibration and flutter analyses were conducted using MSC-Nastran and ZONA 6 module of ZAERO, respectively. Khodaparast et al. [3] used Nastran-based doublet lattice method for aerodynamic modeling to carry out both probabilistic and non-probabilistic flutter analysis of aircraft wing. The wing with spar, ribs, upper and lower skins, and their thickness and area were considered as random variables. For probabilistic analysis, perturbation method and for non-probabilistic analysis, interval and fuzzy logic were used to determine the bounds on the flutter mode. Borello et al. [4] considered both isotropic and composite wing with structural uncertainties for flutter analysis, and the reliability analysis was carried out using various approaches such as First-Order Reliability Method (FORM), Second-Order Reliability Method (SORM), Response Surface Method (RSM), and compared with MCS. Cheng and Xiao [5] proposed a hybrid method based on RSM, Finite Element Method (FEM), and MCS to carry the probabilistic free vibration and flutter analysis of suspension bridge. Castravete and Ibrahim [6] investigated the effect of stiffness uncertainties on flutter of a cantilever wing using MCS and first-order perturbation technique in time domain.

From the literature, it is observed that most of the work reported on probabilistic flutter analysis has been done using commercial software. In the present work, probabilistic flutter analysis of a cantilever wing is carried out using physics-based approach in the frequency domain by considering both bending and torsional rigidity as independent Gaussian random variables. The impetus of the present work is on modeling two-dimensional Theodorson's unsteady aerodynamics [7] in a strip theory approximation containing frequency-dependent terms. In the present first-order perturbation approach, the frequency-dependent aerodynamic terms are also modeled as random variables and their effect on the probabilistic flutter characteristics of the wing is studied.

2 Mathematical Modeling

The Goland wing is a metallic wing [8] and its schematic diagram is shown in Fig. 1. In the figure, points F, G, and H are the aerodynamic center, center of mass, and location of elastic axis at the section, respectively. The dimensionless parameters a and e ($-1 \leq a \leq 1$ and $-1 \leq e \leq 1$) determine the location of elastic axis and inertia axis, respectively, at the section.

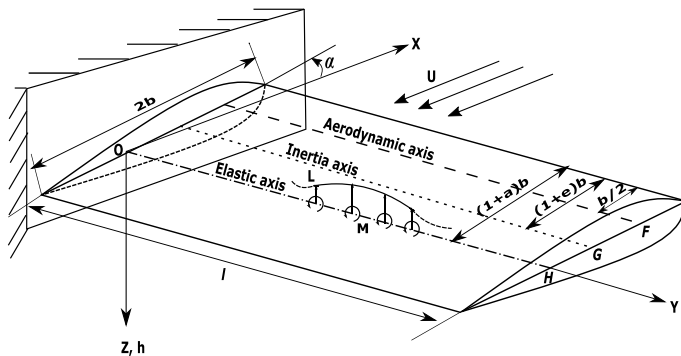The kinetic energy (T) of the wing is defined as

Fig. 1 Schematic representation of cantilever wing (Goland wing)

$$T = \frac{1}{2} \int_0^l I_p \dot{\alpha}^2 dy + \int_0^l m x_\alpha b \dot{h} \dot{\alpha} dy + \frac{1}{2} \int_0^l m \dot{h}^2 dy \tag{1}$$

where I_p, m, b, and $x_\alpha (= e - a)$ are the mass moment of inertia per unit length about elastic axis, mass per unit length of the wing, semi chord of the wing, and dimensionless static unbalance respectively. The $(\dot{)}$ over h and α denotes the time derivatives of heave $h(y, t)$ and pitch displacement $\alpha(y, t)$, respectively.

The potential energy (V) of the wing is expressed as

$$V = \frac{1}{2} \int_0^l EI \left(\frac{\partial^2 h}{\partial y^2} \right)^2 dy + \frac{1}{2} \int_0^l GJ \left(\frac{\partial \alpha}{\partial y} \right)^2 dy \tag{2}$$

The virtual external work done (δW_{ext}) by the system is given as

$$\delta W_{ext} = - \int_0^l L dy \delta h + \int_0^l M dy \delta \alpha \tag{3}$$

where L and $M = (M_{1/4} + L(0.5 + a)b)$ are the lift and moment per unit length, respectively.

Using Hamilton's principle, the governing equations of motion of aeroelastic system can be obtained as

$$m\ddot{h} + m x_\alpha b \ddot{\alpha} + \frac{\partial^2}{\partial y^2} \left(EI \frac{\partial^2 h}{\partial y^2} \right) + L = 0 \tag{4}$$

$$I_p \ddot{\alpha} + m x_\alpha b \ddot{h} - \frac{\partial}{\partial y} \left(GJ \frac{\partial \alpha}{\partial y} \right) - M = 0 \tag{5}$$

According to thin airfoil theory [7], the lift and moment per unit span at the aerodynamic center can be represented as

$$L = 2\pi\rho_\infty b U C(k) \left(U\alpha + \dot{h} + b\left(\frac{1}{2} - a\right)\dot{\alpha}\right) + \pi\rho_\infty b^2 \left(\ddot{h} + U\dot{\alpha} - ba\ddot{\alpha}\right) \quad (6)$$

$$M_{1/4} = -\pi\rho_\infty b^3 \left(\frac{1}{2}\ddot{h} + U\dot{\alpha} + b\left(\frac{1}{8} - \frac{a}{2}\right)\ddot{\alpha}\right) \quad (7)$$

where U is the free stream velocity and $C(k)$ appeared in Eq. 6 is the complex function called Theodorsen's function in which $k(= b\omega/U, \omega$ is the frequency of aeroelastic system) is the reduced frequency. Theodorsen's function is represented for numerical computation as [12]:

$$C(k) = 1 + \frac{0.1757}{1 + (\frac{1.099}{k})} - \frac{0.6724}{1 + (\frac{0.243}{k})} + \left(\frac{2.41}{1 + (\frac{0.214}{k})} - \frac{2.41}{1 + (\frac{0.156}{k})}\right)i \quad (8)$$

The weak form of Eqs. 4 and 5 can be obtained after substituting the expressions of L and M from Eqs. 6 and 7. The elemental Finite Element (FE) equations can be written as

$$M_{sb1}\{\ddot{w}_e\} + EM_{ab1}\{\ddot{w}_e\} + M_{sc1}\{\ddot{\alpha}_e\} + CM_{ac1}\{\ddot{\alpha}_e\} + (B_1 C_{ac1} + B_2 C_{ac1})\{\dot{\alpha}_e\}$$
$$+ DC_{ab1}\{\dot{w}_e\} + AK_{ac1}\{\alpha_e\} + K_{sb1}\{w_e\} = \{F_i\} \quad (9)$$

$$M_{st2}\{\ddot{\alpha}_e\} + RM_{at2}\{\ddot{\alpha}_e\} + M_{sc2}\{\ddot{w}_e\} + TM_{ac2}\{\ddot{w}_e\} + (Q_1 C_{at2} + Q_2 C_{at2})\{\dot{\alpha}_e\}$$
$$+ SC_{ac2}\{\dot{w}_e\} + PK_{ac2}\{\alpha_e\} + K_{st2}\{\alpha_e\} = \{\tau_i\} \quad (10)$$

In Eqs. 9 and 10, $\{w_e\}$ and $\{\alpha_e\}$ are elemental bending and torsional degrees-of-freedom, respectively, and $\{F_i\}$ and $\{\tau_i\}$ are the internal load vectors, respectively. The terms appearing in Eq. 9 can be written as

$$M_{sb1} = m \int_{y_i}^{y_{i+1}} \{N_w\}\lfloor N_w \rfloor dy$$

$$EM_{ab1} = \pi\rho_\infty b^2 \int_{y_i}^{y_{i+1}} \{N_w\}\lfloor N_w \rfloor dy$$

$$M_{sc1} = mx_\alpha b \int_{y_i}^{y_{i+1}} \{N_w\}\lfloor N_\alpha \rfloor dy$$

$$CM_{ac1} = -\pi\rho_\infty b^3 a \int_{y_i}^{y_{i+1}} \{N_w\}\lfloor N_\alpha \rfloor dy$$

$$B_1 C_{ac1} = U C(k)\pi\rho_\infty b^2 (1 - 2a) \int_{y_i}^{y_{i+1}} \{N_w\}\lfloor N_\alpha \rfloor dy \quad (11)$$

$$B_2 C_{ac1} = U\pi\rho_\infty b^2 \int_{y_i}^{y_{i+1}} \{N_w\} \lfloor N_\alpha \rfloor dy$$

$$DC_{ab1} = UC(k)2\pi\rho_\infty b \int_{y_i}^{y_{i+1}} \{N_w\} \lfloor N_w \rfloor dy$$

$$AK_{ac1} = U^2 C(k)2\pi\rho_\infty b \int_{y_i}^{y_{i+1}} \{N_w\} \lfloor N_\alpha \rfloor dy$$

$$K_{sb1} = EI \int_{y_i}^{y_{i+1}} \{N_w''\} \lfloor N_w'' \rfloor dy$$

and the terms in Eq. 10 can be written as

$$M_{st2} = I_p \int_{y_i}^{y_{i+1}} \{N_\alpha\} \lfloor N_\alpha \rfloor dy$$

$$RM_{at2} = \pi\rho_\infty b^4 \left(a^2 + \frac{1}{8}\right) \int_{y_i}^{y_{i+1}} \{N_\alpha\} \lfloor N_\alpha \rfloor dy$$

$$M_{sc2} = m x_\alpha b \int_{y_i}^{y_{i+1}} \{N_\alpha\} \lfloor N_w \rfloor dy$$

$$TM_{ac2} = -\pi\rho_\infty b^3 a \int_{y_i}^{y_{i+1}} \{N_\alpha\} \lfloor N_w \rfloor dy$$

$$Q_1 C_{at2} = -UC(k)\pi\rho_\infty b^3 \left(\frac{1}{2} + a\right)(1 - 2a) \int_{y_i}^{y_{i+1}} \{N_\alpha\} \lfloor N_\alpha \rfloor dy \qquad (12)$$

$$Q_2 C_{at2} = -U\pi\rho_\infty b^3 \left(-\frac{1}{2} + a\right) \int_{y_i}^{y_{i+1}} \{N_\alpha\} \lfloor N_\alpha \rfloor dy$$

$$SC_{ac2} = -UC(k)2\pi\rho_\infty b^2 \left(\frac{1}{2} + a\right) \int_{y_i}^{y_{i+1}} \{N_\alpha\} \lfloor N_w \rfloor dy$$

$$PK_{ac2} = -U^2 C(k)2\pi\rho_\infty b^2 \left(\frac{1}{2} + a\right) \int_{y_i}^{y_{i+1}} \{N_\alpha\} \lfloor N_\alpha \rfloor dy$$

$$K_{st2} = GJ \int_{y_i}^{y_{i+1}} \{N_\alpha'\} \lfloor N_\alpha' \rfloor dy$$

where N_w and N_α are the bending and torsional shape functions, and $(')$ represents the derivative with respect to y. Now assembling the elemental form of Eqs. 9 and 10, we get the assembled form of FE equation as

$$([M_s] + [M_a])\{\ddot{q}\} + (U[C_a] + UC(k)[C_{a\omega}])\{\dot{q}\}$$
$$+ ([K_b] + [K_t] + U^2 C(k)[K_{a\omega}])\{q\} = \{0\} \quad (13)$$

In Eq. 13, the displacement vector $\{q\}$ contains all bending and torsional degrees-of-freedom. $[M_s]$, $[M_a]$, $U[C_a]$, $[K_b]$, and $[K_t]$ are the structural inertia, aerodynamic inertia, aerodynamic damping, bending stiffness, and torsional stiffness matrices, respectively, and $UC(k)[C_{a\omega}]$ and $U^2 C(k)[K_{a\omega}]$ are frequency-dependent damping and stiffness matrices respectively. Let $\{q\}$ be represented by harmonic function $\{q\} = \{\bar{q}\}e^{\lambda t}$, where $\lambda = -\zeta\omega + i\omega$ and in other form $\lambda = \lambda_R + i\lambda_I$, and substituting it in Eq. 13 gives the following expression as

$$\left[\lambda^2 ([M_s] + [M_a]) + \lambda (U[C_a] + UC(k)[C_{a\omega}])\right.$$
$$\left. + ([K_b] + [K_t] + U^2 C(k)[K_{a\omega}])\right]\{\bar{q}\} = \{0\} \quad (14)$$

The above equation can be solved using state-space approach as an eigenvalue problem.

3 Stochastic Modeling

The stochastic modeling of the geometrically coupled cantilever wing is based on first-order perturbation approach. In this approach, the random variables are expanded using Taylor's series as

$$\beta = \beta_o + \frac{\partial\beta}{\partial r}|_{r=r_o}\delta r \quad (15)$$

where β_o is the mean of random variables and r denotes independent random parameters. The derivatives of the random variables are evaluated at the mean value of the random variables. In the present problem, both bending rigidity and torsional rigidity are considered as Gaussian random variables. The random bending stiffness, torsional stiffness, eigenvalue, eigenvector, and frequency-dependent Theodorsen's function expanded via Taylor's series truncated to first order term can be written as

$$[K_b] = [K_b^o] + \frac{\partial[K_b]}{\partial r}|_{r=r_o}\delta r$$

$$[K_t] = [K_t^o] + \frac{\partial[K_t]}{\partial r}|_{r=r_o}\delta r$$

$$\lambda = \lambda^o + \frac{\partial \lambda}{\partial r}|_{r=r_o} \delta r \tag{16}$$

$$\{\bar{q}\} = \{\bar{q}^o\} + \frac{\partial \{\bar{q}\}}{\partial r}|_{r=r_o} \delta r$$

$$C(k) = C(k^o) + \frac{b}{U} \left(\frac{\partial C(k)}{\partial k} \frac{\partial \lambda_I}{\partial r} \right)|_{r=r_o} \delta r$$

Now substituting terms from Eq. 16 to Eq. 14 and separating zeroth-order and first-order terms:

Zeroth order:

$$\left[(\lambda^o)^2 \left([M_s] + [M_a] \right) + \lambda^o \left(U [C_a] + U C(k^o) [C_{a\omega}] \right) \right.$$
$$\left. + \left(\left[K_b^o \right] + \left[K_t^o \right] + U^2 C(k^o) [K_{a\omega}] \right) \right] \{\bar{q}^o\} = \{0\} \tag{17}$$

First order:

$$\left[(\lambda^o)^2 \left([M_s] + [M_a] \right) + \lambda^o \left(U [C_a] + U C(k^o) [C_{a\omega}] \right) \right.$$
$$\left. + \left(\left[K_b^o \right] + \left[K_t^o \right] + U^2 C(k^o) [K_{a\omega}] \right) \right] \frac{\partial \{\bar{q}\}}{\partial r}$$
$$+ \frac{\partial \lambda}{\partial r} \left[2\lambda^o \left([M_s] + [M_a] \right) + U [C_a] + U C(k^o) [C_{a\omega}] \right] \{\bar{q}^o\}$$
$$+ \frac{\partial \lambda_I}{\partial r} \left[\frac{b}{U} \frac{\partial C(k)}{\partial k} \lambda^o U [C_{a\omega}] + \frac{b}{U} \frac{\partial C(k)}{\partial k} U^2 [K_{a\omega}] \right] \{\bar{q}^o\}$$
$$= - \left(\frac{\partial [K_b]}{\partial r} + \frac{\partial [K_t]}{\partial r} \right) \{\bar{q}^o\} \tag{18}$$

Now multiplying Eq. 18 by adjoint eigenvector or left eigenvector transpose $\{\bar{X}_{adj}\}^T$ [9–11], we get the following equation as:

$$\{\bar{X}_{adj}\}^T \left[(\lambda^o)^2 \left([M_s] + [M_a] \right) + \lambda^o \left(U [C_a] + U C(k^o) [C_{a\omega}] \right) \right.$$
$$\left. + \left(\left[K_b^o \right] + \left[K_t^o \right] + U^2 C(k^o) [K_{a\omega}] \right) \right] \frac{\partial \{\bar{q}\}}{\partial r}$$
$$+ \frac{\partial \lambda}{\partial r} \{\bar{X}_{adj}\}^T \left[2\lambda^o \left([M_s] + [M_a] \right) + U [C_a] + U C(k^o) [C_{a\omega}] \right] \{\bar{q}^o\}$$
$$+ \frac{\partial \lambda_I}{\partial r} \{\bar{X}_{adj}\}^T \left[\frac{b}{U} \frac{\partial C(k)}{\partial k} \lambda^o U [C_{a\omega}] + \frac{b}{U} \frac{\partial C(k)}{\partial k} U^2 [K_{a\omega}] \right] \{\bar{q}^o\}$$
$$= -\{\bar{X}_{adj}\}^T \left(\frac{\partial [K_b]}{\partial r} + \frac{\partial [K_t]}{\partial r} \right) \{\bar{q}^o\} \tag{19}$$

The eigenvector derivative coefficient matrix in Eq. 19 becomes zero. Equation 19 can be rewritten as

$$
\frac{\partial \lambda}{\partial r} \{\bar{X}_{adj}\}^T \left[2\lambda^o \left([M_s] + [M_a]\right) + U[C_a] + UC(k^o)[C_{a\omega}] \right] \{\bar{q}^o\}
$$

$$
+ \frac{\partial \lambda_I}{\partial r} \{\bar{X}_{adj}\}^T \left[\frac{b}{U} \frac{\partial C(k)}{\partial k} \lambda^o U[C_{a\omega}] + \frac{b}{U} \frac{\partial C(k)}{\partial k} U^2 [K_{a\omega}] \right] \{\bar{q}^o\}
$$

$$
= -\{\bar{X}_{adj}\}^T \left(\frac{\partial [K_b]}{\partial r} + \frac{\partial [K_t]}{\partial r} \right) \{\bar{q}^o\} \quad (20)
$$

Substituting complex form of eigenvalue ($\lambda = \lambda_R + i\lambda_I$) in Eq. 20 and solving for real and imaginary part of eigenvalue derivatives as

$$
\frac{\partial \lambda_R}{\partial r} = \frac{\phi(\gamma - \varphi) - \eta(\psi + \xi)}{\varphi(\gamma - \varphi) - \xi(\psi + \xi)} \quad (21)
$$

$$
\frac{\partial \lambda_I}{\partial r} = \frac{\eta\varphi - \phi\xi}{\varphi(\gamma - \varphi) - \xi(\psi + \xi)} \quad (22)
$$

where terms $\xi, \varphi, \gamma, \psi, \eta$ and ϕ can be obtained from the expression given below:

$$
\xi + i\varphi = \{\bar{X}_{adj}\}^T \left[2\lambda^o \left([M_s] + [M_a]\right) + U[C_a] + UC(k^o)[C_{a\omega}] \right] \{\bar{q}^o\}
$$

$$
\gamma + i\psi = \{\bar{X}_{adj}\}^T \left[\frac{b}{U} \frac{\partial C(k)}{\partial k} \lambda^o U[C_{a\omega}] + \frac{b}{U} \frac{\partial C(k)}{\partial k} U^2 [K_{a\omega}] \right] \{\bar{q}^o\} \quad (23)
$$

$$
\eta + i\phi = -\{\bar{X}_{adj}\}^T \left(\frac{\partial [K_b]}{\partial r} + \frac{\partial [K_t]}{\partial r} \right) \{\bar{q}^o\}
$$

The variance of the real part and imaginary part can be obtained as

$$
Var(\lambda_R) = \left(\frac{\partial \lambda_R}{\partial r} \right)^2 Var(r) \quad (24)
$$

$$
Var(\lambda_I) = \left(\frac{\partial \lambda_I}{\partial r} \right)^2 Var(r) \quad (25)
$$

where variance of λ_I also represents variance of frequency (ω).

4   Results and Discussion

First, the mean flutter analysis of the wing is performed using zeroth-order equation based on *pk* method using the mean data given in Table 1. Figure 2 shows the variation of mean damping (λ_R^o) and frequency (λ_I^o) of the wing at various free stream velocity U. From the figure, the mean flutter velocity is found to be 137.38 m/s, which matches well with those given in [12].

Table 1   Properties of Goland wing [12]

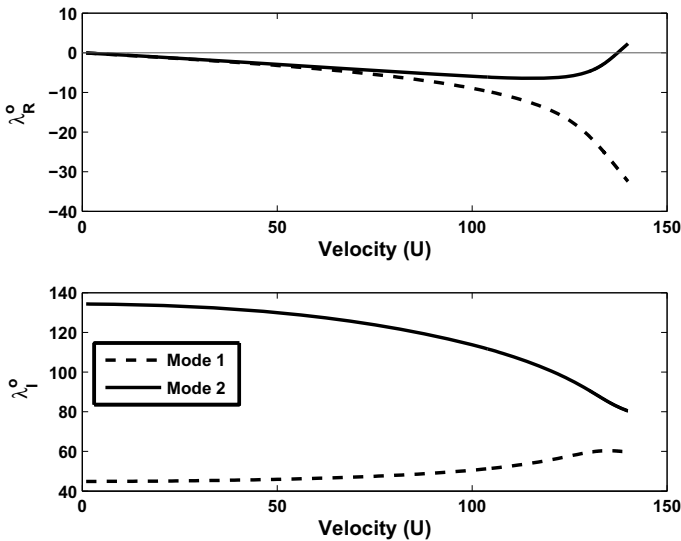| Parameters	Description	Values
EI	Span-wise bending stiffness	9.77×10^6 Nm^2
GJ	Span-wise torsion stiffness	0.988×10^6 Nm^2
m	Mass per unit span	35.719 Kg/m
x_α	Dimensionless static unbalance	0.33
a	Elastic axis location parameter	-0.2
b	Semi-reference chord	0.9144 m
l	Span	6.09 m
I_p	Mass moment of inertia per unit span	6.5704 Kgm^2/m
ρ_∞	Free stream density	1.225 Kg/m^3

Fig. 2   Variation of real and imaginary part of mean eigenvalue with free stream velocity (U)

Table 2 Variation of mean and SD of eigenvalues with free stream velocity for COV of $EI = 0.05$

Velocity U (m/s)	Perturbation approach				Monte Carlo Simulation (with 10,000 Samples)			
	Mean (λ_R^o)	Mean (λ_I^o)	SD (λ_R)	SD (λ_R^o)	Mean (λ_I)	Mean (λ_I^o)	SD (λ_R)	SD (λ_I)
Mode 1								
100	−8.9547	50.5290	0.0276	0.9734	−8.9568	50.5050	0.0275	0.9741
125	−17.0811	57.6563	0.0424	0.9228	−17.0839	57.6268	0.0415	0.9242
135	−26.4397	60.3614	0.0346	0.8351	−26.4374	60.3338	0.0364	0.8369
Mode 2								
100	−5.9584	113.8010	0.0928	0.4779	−5.9591	113.8010	0.0927	0.4779
125	−5.9187	96.2131	0.1907	0.5428	−5.9215	96.2191	0.1904	0.5427
135	−1.9540	84.9500	0.2509	0.7361	−1.9678	84.9576	0.2516	0.7346

The probabilistic flutter analysis of cantilever wing is performed by treating EI and GJ as stochastically independent Gaussian random variables with 5% COV in EI and GJ. The mean and Standard Deviation (SD) of the first two eigenvalues obtained using first-order perturbation approach and MCS are shown in Tables 2 and 3, respectively. From the tables, it is observed that the mean and SD of eigenvalues obtained using the perturbation approach matches well with MCS at various free stream velocities which validate the present first-order perturbation approach for probabilistic analysis. From the tables, it is also observed that there is an increasing trend of SD of damping (real part) for second eigenmode (flutter mode) with increasing velocity, which indicates that eigenmodes are sensitive to probabilistic variations which can have an influence on the design of aircraft with proper flutter margin. Comparing the SD of the real part for both mode 1 and mode 2, the standard deviation of mode 2 is greater than mode 1 corresponding to a particular velocity

Table 3 Variation of mean and SD of eigenvalues with free stream velocity for COV of $GJ = 0.05$

| Velocity U (m/s)	Perturbation approach				Monte Carlo Simulation (with 10,000 Samples)			
	Mean (λ_R^o)	Mean (λ_I^o)	SD (λ_R)	SD (λ_I)	Mean (λ_R^o)	Mean (λ_I^o)	SD (λ_R)	SD (λ_I)
Mode 1								
100	−8.9547	50.5290	0.2654	0.1501	−8.9787	50.5406	0.2729	0.1528
125	−17.0811	57.6563	1.5942	0.7578	−17.3649	57.6105	1.7244	0.6612
135	−26.4397	60.3614	3.2967	0.6939	−26.5630	59.9716	3.1417	0.8463
Mode 2								
100	−5.9584	113.8010	0.1154	3.6420	−5.9461	113.7181	0.1198	3.6478
125	−5.9187	96.2131	0.7781	4.9591	−5.7294	96.0161	0.9259	4.9599
135	−1.9540	84.9500	2.8628	5.1211	−1.6325	85.2785	2.6318	4.8720
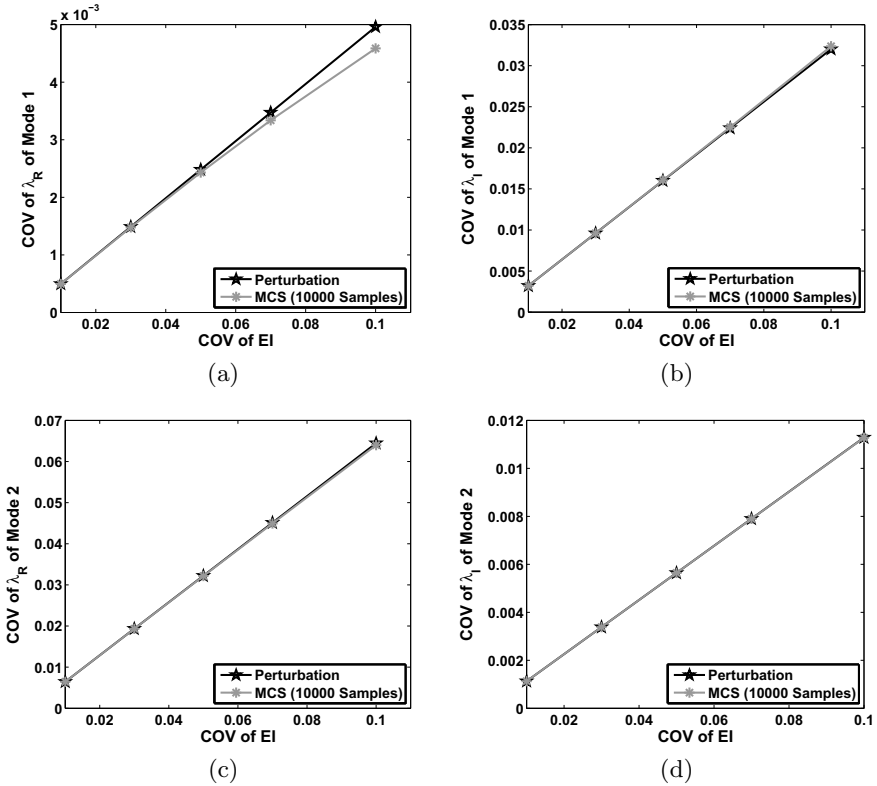
Fig. 3 COV of real and imaginary part of eigenvalues of various modes for different COV of bending rigidity at U = 125 m/s **a** λ_R of mode 1, **b** λ_I of mode 1, **c** λ_R of mode 2, and **d** λ_I of mode 2

for the variation in bending rigidity and mode 1 in the case of variation in torsional rigidity. This means that uncertainty in bending rigidity affects the real part of mode 2 whereas torsional uncertainty affects the real part of mode 1.

Figure 3 shows the variations in the real and imaginary part of eigenvalues for different COV of EI at velocity 125 m/s and a very good agreement with MCS is observed. The COV follows a linear relationship for most of the cases except for λ_R of the first mode, which starts significantly deviating after 7% COV of EI.

Figure 4 shows the variation in the real and imaginary part of eigenvalues at a free stream velocity of 125 m/s for different COV of GJ. From the figure, it can be observed that the COV of λ_R of mode 1, mode 2, and λ_I of mode 1 are accurate up to 3% of COV of GJ, and λ_I of mode 2 is accurate for all value of COV of GJ. A linear relationship between COV of eigenvalues up to 3% COV of GJ can be also observed.

Figure 5 shows the COV of real and imaginary part of eigenvalues at various free stream velocities due to variation in EI and GJ. From the figure, it can be observed
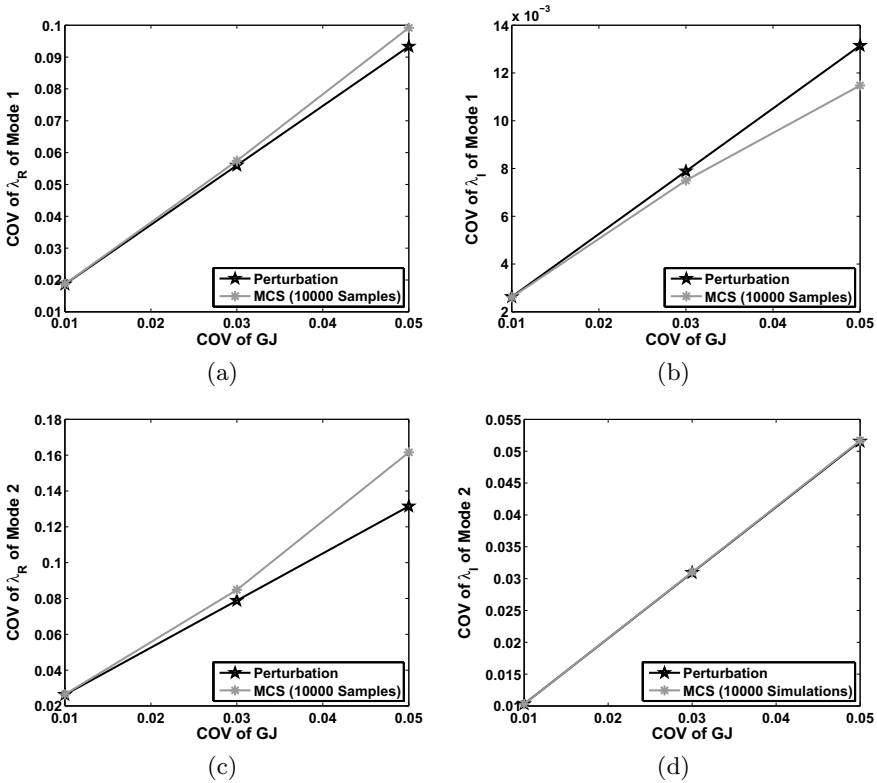
Fig. 4 COV of real and imaginary part of eigenvalues of various modes for different COV of torsional rigidity at $U = 125$ m/s **a** λ_R of mode 1, **b** λ_I of mode 1, **c** λ_R of mode 2, and **d** λ_I of mode 2

that the COV of λ_R for mode 2 has very high value near to flutter velocity due to variation in EI and GJ. It is also observed that the COV of λ_I due to bending rigidity uncertainty is low for mode 2 in comparison with torsional rigidity uncertainty. This may be due to the fact that eigenvalues are more sensitive due to variation in torsional rigidity near to flutter velocity. Since mode 2 is the flutter mode, we further investigate the probability density function (*pdf*) of second mode at various velocities.

Figure 6 shows the *pdf* of real and imaginary part of eigenvalues for COV of EI (= 0.05) at 125 m/s and 137 m/s obtained from MCS with 10,000 simulations. From the figure, it is observed that the *pdf* of λ_R of mode 2 at velocity 137 m/s is slightly skewed than at velocity 125 m/s. It is also observed that λ_I of mode 2 at velocity 137 m/s shows a wider band than at velocity 125 m/s.

Figure 7 shows the *pdf* of real and imaginary part of eigenvalues for COV of GJ (= 0.05) at 125 m/s and 137 m/s obtained from MCS with 10,000 simulations. From the figure, it is observed that the *pdf* of λ_R of mode 2 at velocity 137 m/s shows a wider band than at velocity 125 m/s. The *pdf* of λ_R at velocity 137 m/s indicates

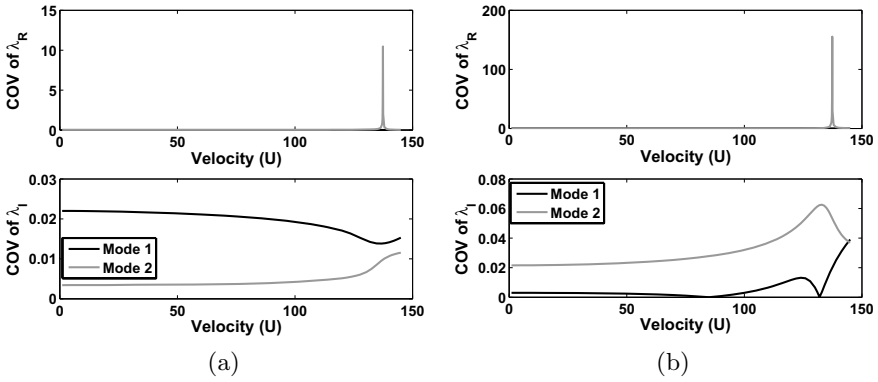**Fig. 5** COV of real and imaginary part of eigenvalues at various free stream velocities due to **a** COV of $EI = 0.05$, **b** COV of $GJ = 0.05$
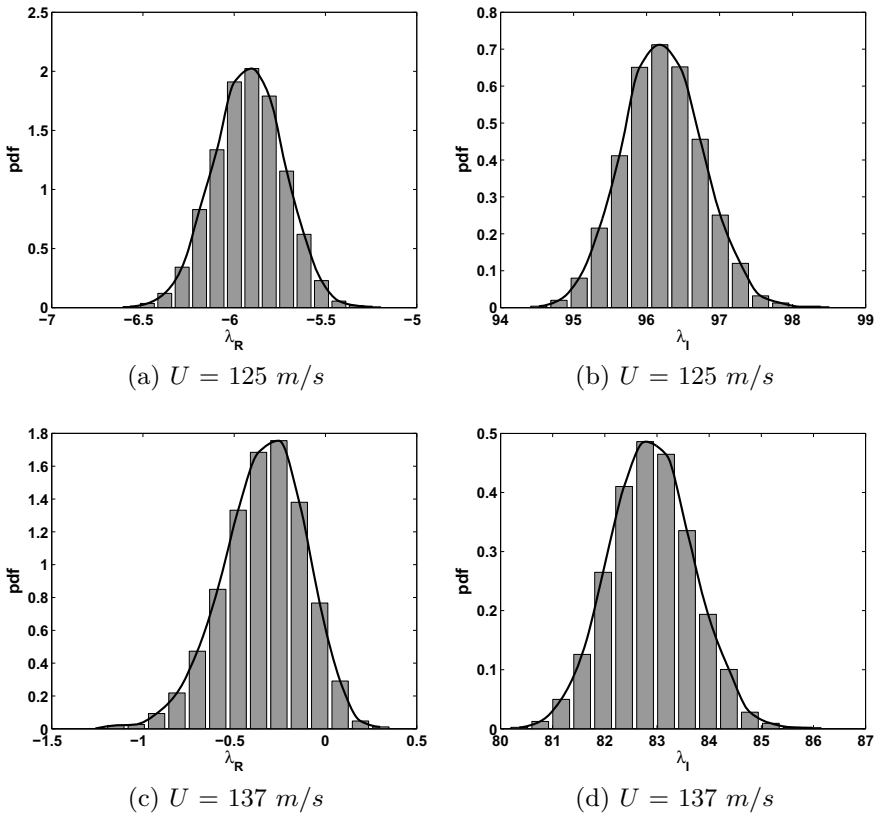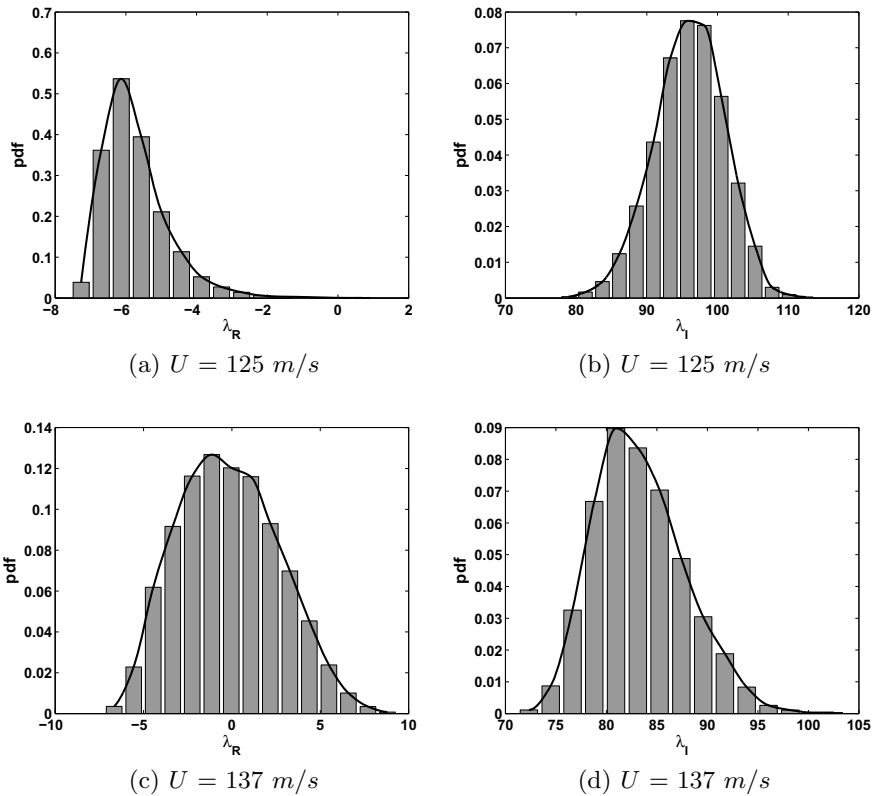

Fig. 6 pdfs of real and imaginary part of eigenvalue of mode 2 for COV of $EI = 0.05$ **a** λ_R at $U = 125$ m/s, **b** λ_I at $U = 125$ m/s, **c** λ_R at $U = 137$ m/s, and **d** λ_I at $U = 137$ m/s

(a) $U = 125\ m/s$

(b) $U = 125\ m/s$

(c) $U = 137\ m/s$

(d) $U = 137\ m/s$

Fig. 7 pdfs of real and imaginary part of eigenvalue of mode 2 for COV of GJ = 0.05 **a** λ_R at U = 125 m/s, **b** λ_I at U = 125 m/s, **c** λ_R at U = 137 m/s, and **d** λ_I at U = 137 m/s

that there is a chance of occurrence of flutter due to uncertainties in the bending and torsional rigidities as seen in Figs. 6c and 7c (+ ve region under *pdf* of λ_R). The figures also indicate that chances of occurrence of flutter is high in the case of variation in GJ as compared to EI due to large positive area under *pdf* of λ_R of mode 2.

5 Conclusions

The probabilistic flutter analysis of geometrically coupled cantilever wing has been carried out using first order perturbation approach considering bending rigidity and torsional rigidity as Gaussian random variables. The probabilistic response of the wing has been obtained in terms of mean and SD of the real and imaginary part

of eigenvalues for different COV of random variables at a particular velocity using the perturbation approach. The results are compared with MCS and found to be in very good agreement for variation in EI for all COV considered. In the case of the variation in GJ, the results show accuracy up to 3% COV in GJ beyond which it loses its accuracy, which limits the applicability of perturbation approach. From the results obtained, we can conclude that the COV of λ_R of the flutter mode near the flutter velocity starts increasing, and theoretically becomes infinite at the flutter velocity. The *pdf* of λ_R for flutter mode shows that there are chances of occurrence of flutter at lower velocities in the presence of uncertainties. Hence, consideration of uncertainties is very important in the design of the aircraft for proper flutter margin.

References

1. Pettit CL (2004) Uncertainty quantification in aeroelasticity: recent results and research challenges. J Aircraft 41(5):1217–1229. https://doi.org/10.2514/1.3961
2. Kurdi M, Lindsley N, Beran P (2007) Uncertainty quantification of the Goland$^+$ wing's flutter boundary. In: AIAA atmospheric flight mechanics and exhibit, hilton head, South Carolina, 20–23 August 2007. https://doi.org/10.2514/6.2007-6309
3. Khodaparast H, Mottershead J, Badcock K (2010) Propagation of structural uncertainty to linear aeroelastic stability. Comput Struct 88(3-4):223–236. https://doi.org/10.1016/j.compstruc.2009.10.005
4. Borello F, Cestino E, Frulla G (2010) Structural uncertainty effect on classical wing flutter characteristics. J Aerospace Eng 23(4):327–338. https://doi.org/10.1061/(ASCE)AS.1943-5525.0000049
5. Cheng J, Xiao RC (2005) Probabilistic free vibration and flutter analyses of suspension bridges. Eng Struct 27(10):1509–1518. https://doi.org/10.1016/j.engstruct.2005.03.016
6. Castravete SC, Ibrahim RA (2008) Effect of stiffness uncertainties on the flutter of a cantilever wing. AIAA J 46(4):925–935. https://doi.org/10.2514/1.31692
7. Theodorsen T (1935) General theory of aerodynamic instability and the mechanism of flutter. Tech. Rep, NACA, p 496
8. Goland M, Buffalo N (1945) The flutter of a uniform cantilever wing. J Appl Mech-T ASME 12(4):A197–A208
9. Nelson RB (1976) Simplified calculation of eigenvector derivatives. AIAA J 14(9):1201–1205. https://doi.org/10.2514/3.7211
10. Ji-ming L, Wei W (1987) First-order perturbation solution to the complex eigenvalues. Appl Math Mech 8(6):509–514. https://doi.org/10.1007/BF02017399
11. Adhikari S (1999) Rates of change of eigenvalues and eigenvectors in damped dynamic system. AIAA J 37(11):1452–1458. https://doi.org/10.2514/2.622
12. Irani S, Sazesh S (2013) A new flutter speed analysis method using stochastic approach. J Fluid Struct 40:105–114. https://doi.org/10.1016/j.jfluidstructs.2013.03.018